Received: 9 June 2022 | Revised: 22 January 2023 | Accepted: 16 September 2023

DOI: 10.1111/jnc.15977

Journal of Neurochemistry JNC The Official Journal of the International Society for Neurochemistry WILEY

ORIGINAL ARTICLE

Neuronal NADPH oxidase is required for neurite regeneration of *Aplysia* bag cell neurons

S. M. Sabbir Alam[1] | Yuichiro Watanabe[2] | Brooke L. Steeno[2] | Soumyajit Dutta[1] | Halie A. Szilagyi[1] | Alexander Wei[2,3] | Daniel M. Suter[1,3,4,5,6]

[1]Department of Biological Sciences, Purdue University, West Lafayette, Indiana, USA

[2]Department of Chemistry, Purdue University, West Lafayette, Indiana, USA

[3]Birck Nanotechnology Center, Purdue University, West Lafayette, Indiana, USA

[4]Purdue Institute for Integrative Neuroscience, Purdue University, West Lafayette, Indiana, USA

[5]Purdue Institute for Inflammation, Immunology, and Infectious Disease, Purdue University, West Lafayette, Indiana, USA

[6]Bindley Bioscience Center, Purdue University, West Lafayette, Indiana, USA

Correspondence
Daniel M. Suter, Department of Biological Sciences, Purdue University, 915 Mitch Daniels Boulevard, West Lafayette, IN 47907-2054, USA.
Email: dsuter@purdue.edu

Present address
Yuichiro Watanabe, Department of Polymer Chemistry, Kyoto University, Kyoto, Japan

Funding information
American Chemical Society Petroleum Research Fund, Grant/Award Number: 58453-ND4; Indiana Spinal Cord & Brain Injury Research Fund, Grant/Award Number: Contract 26351; Japan Society for the Promotion of Science; National Institute of Neurological Disorders and Stroke, Grant/Award Number: 5R01NS117701

Abstract

NADPH oxidase (Nox), a major source of reactive oxygen species (ROS), is involved in neurodegeneration after injury and disease. Nox is expressed in both neuronal and non-neuronal cells and contributes to an elevated ROS level after injury. Contrary to the well-known damaging effect of Nox-derived ROS in neurodegeneration, recently a physiological role of Nox in nervous system development including neurogenesis, neuronal polarity, and axonal growth has been revealed. Here, we tested a role for neuronal Nox in neurite regeneration following mechanical transection in cultured *Aplysia* bag cell neurons. Using a novel hydrogen peroxide (H_2O_2)-sensing dye, 5′-(*p*-borophenyl)-2′-pyridylthiazole pinacol ester (BPPT), we found that H_2O_2 levels are elevated in regenerating growth cones following injury. Redistribution of Nox2 and $p40^{phox}$ in the growth cone central domain suggests Nox2 activation after injury. Inhibiting Nox with the pan-Nox inhibitor celastrol reduced neurite regeneration rate. Pharmacological inhibition of Nox is correlated with reduced activation of Src2 tyrosine kinase and F-actin content in the growth cone. Taken together, these findings suggest that Nox-derived ROS regulate neurite regeneration following injury through Src2-mediated regulation of actin organization in *Aplysia* growth cones.

KEYWORDS
growth cone, hydrogen peroxide, NADPH oxidase, neurite regeneration, reactive oxygen species

Abbreviations: ASW, artificial sea water; BPPT, 5′-(*p*-borophenyl)-2′-pyridylthiazole pinacol ester; C, central; CNS, central nervous system; CRO, calcein red orange; CST, celastrol; DIC, differential interference contrast; DMSO, dimethylsulfoxide; DRG, dorsal root ganglion; NADPH, nicotinamide adenine dinucleotide phosphate; Nox, NADPH oxidase; P, peripheral; PL, photoluminescence; ROS, reactive oxygen species; SCI, spinal cord injury; T, transition.

1 | INTRODUCTION

Nox family proteins are membrane-bound enzymes that transfer electrons from NADPH to oxygen and thereby produce superoxide or hydrogen peroxide (H_2O_2) (Bedard & Krause, 2007; Magnani et al., 2017). Classically known for its role in reactive oxygen species (ROS)-mediated killing of pathogens by phagocytic cells, Nox has later been implicated in cell proliferation, differentiation, and physiology (Bedard & Krause, 2007; Moghadam et al., 2021). The Nox family contains seven subfamilies with different isoforms that share common structural motifs but exhibit distinct cellular expression patterns and activation mechanisms (Kawahara et al., 2007). The fully activated Nox2 complex consists of two membrane proteins, Nox2/gp91^{phox} and p22^{phox}, three cytosolic subunits, p47^{phox}, p67^{phox}, and p40^{phox}, and the small G protein Rac (Brandes et al., 2014; Rastogi et al., 2017). Nox1–4 as well as associated cytosolic subunits are expressed in different types of neurons and glial cells (Nayernia et al., 2014; Terzi & Suter, 2020). Different Nox isoforms have a role in various aspects of nervous system development including in neurogenesis, neuronal polarity, axonal growth, and guidance (Terzi et al., 2021; Terzi & Suter, 2020; Wilson et al., 2018).

Elevated levels of Nox expression and activation as well as increased ROS concentrations have been associated with nervous system injury including traumatic brain and spinal cord injury (SCI) (Cooney et al., 2014; Lee et al., 2021; von Leden et al., 2017; Xu et al., 2005). Neuronal damage occurs not only by primary mechanical injury but also by secondary inflammation and ROS-mediated oxidative stress (Ahuja et al., 2017; Anjum et al., 2020). Nox inhibition after SCI improved functional recovery in animal models (Impellizzeri et al., 2011; Sun et al., 2017); however, antioxidant treatments for human SCI patients had very limited success so far (Hall, 2011). This raises the question as to whether an intermediate level of Nox activity and ROS is required for optimal axonal regeneration like in normal development, whereas too high levels of Nox activity and ROS as found in neurological diseases and trauma are detrimental (Terzi & Suter, 2020). Indeed, there is evidence that physiological levels of H_2O_2 and Nox activity are needed for axonal regeneration. Fin amputation in zebrafish larvae resulted in initial denervation and significant H_2O_2 production at the wound site, which in turn supported axonal growth and re-innervation of peripheral axons at the injury site (Rieger & Sagasti, 2011). Similarly, H_2O_2 promotes peripheral axonal regeneration following fin amputation in adult zebrafish involving a positive feedback loop between H_2O_2 and nerve regeneration (Meda et al., 2016). Since both neuronal and glial cells are involved in axonal regeneration, the specific cellular source of Nox and ROS contributing to regeneration has typically not been determined, especially for in vivo studies. Di Giovanni and co-workers provided some insights into the cellular sources of Nox involved in axonal regeneration using the mouse conditioned lesioning system (De Virgiliis et al., 2020; Hervera et al., 2018). Regeneration of injured dorsal root ganglion (DRG) sensory neurons and sciatic nerve was enhanced by Nox2 delivered to injured axons by exosomes derived from macrophages that were recruited to the injury site (Hervera et al., 2018). Combining environmental enrichment with conditioned lesioning resulted in a up-regulation of Nox2 expression in mouse DRG neurons, which enhanced axonal regeneration of sensory neurons following SCI (De Virgiliis et al., 2020). To determine whether neuronal Nox-derived H_2O_2 is required for neurite regeneration following injury, here, we have used the well-defined and controlled in vitro culture system of *Aplysia* bag cell neurons.

One of the challenges in the field of ROS signaling is the reliable detection and quantification of H_2O_2 in live cells, as just a few suitable probes are available (Sies et al., 2022). Boronate-based fluorescent dyes are one of the most effective probes for the detection of H_2O_2 (Sikora et al., 2020). Aryl boronates are converted selectively by hydroperoxides and peroxyanions into phenolic products on timescales that are well suited for biological imaging (Lippert et al., 2011; Zielonka et al., 2012). Early examples of aryl boronate dyes such as peroxyfluor-1 (PF1) are able to detect oxidative stress in cells induced by exogenous H_2O_2 (Chang et al., 2004; Lippert et al., 2011); however, the limited sensitivity of these dyes make detection of endogenous H_2O_2 levels under physiological conditions challenging. Second generation boronate dyes such as peroxyfluor-6 acetoxymethyl ester (PF6-AM) benefit from increased cellular retention and sensitivity (Dickinson et al., 2011; Lippert et al., 2011; Munnamalai et al., 2014); however, no reliable commercial sources of high-quality PF6-AM were available when we initiated this project. For this reason, we developed a novel, highly emissive boronate-based redox probe, 5′-(*p*-borophenyl)-2′-pyridylthiazole pinacol ester (BPPT, **1**), as an intracellular H_2O_2-sensing probe.

This study addresses the question whether neuronal Nox is required for the regeneration of neurites developed by *Aplysia* bag cell neurons following a mechanical transection. Based on the NCBI protein database, *Aplysia californica* has four different Nox isoforms: Nox2, Nox5-like, Duox, and Duox2. Previously, we reported on Nox2 expression in *Aplysia* growth cones and the role of Nox-derived H_2O_2 in neurite outgrowth (Munnamalai et al., 2014; Munnamalai & Suter, 2009). Here, we found that regenerating growth cones have higher H_2O_2 levels and Nox2 activity compared to control growth cones that were not transected. Furthermore, pharmacological inhibition of Nox reduced the growth rate of regenerating neurites as well as the F-actin content and Src2-activation state in regenerating growth cones. In summary, our results show that neuronal Nox is required for neurite regeneration following injury.

2 | MATERIALS AND METHODS

2.1 | Aplysia bag cell neuronal culture

Aplysia bag cell ganglia were collected from adult (100–150 g) *A. californica* purchased from Marinus Scientific or from the National Resource for *Aplysia*, University of Miami. Bag cell neurons were cultured using protocol described previously (Suter, 2011). Briefly, $MgCl_2$ solution (0.5 M) was injected into the *Aplysia* body cavity for anesthetization. Animals were then dissected to open the body cavity to collect the abdominal ganglion. The ganglion was digested overnight (15–16 h) using 10 mg/mL dispase II (cat. no. D4693,

Sigma) in L-15 medium (cat. no. 41300039, Thermo Fisher Scientific) supplemented with artificial sea water (ASW, pH 7.8). Bag cell neurons were collected from the bag cell cluster through separation by mechanical force (Suter, 2011). Bag cell neurons were plated onto coverslips coated with 20 μg/mL poly-L-lysine (70–150 kD) (cat. no. P6282, Sigma) diluted with hemolymph (Athamneh et al., 2017). L-15 medium supplemented with ASW was used as the culture medium. Culture dishes were kept in the incubator (14°C) for 24–48 h before imaging or in vitro transection was performed. Culture and experimental conditions were uniformly maintained throughout the study, and no blinding of experimental treatments was implemented. As we used an invertebrate animal model for collection of neuronal cells, no institutional ethics approval was required.

2.2 | In vitro neurite transection and regeneration

Bag cell neurons cultured for 48 h were mounted into a custom-made open chamber to perform in vitro neurite transection and observe neurite regeneration after mechanical injury (Suter, 2011). Therefore, we pulled glass capillaries (cat. no. 2-000-001, Drummond Scientific Company) with a Narishige PP830 vertical pipette puller to achieve microneedles with tip diameter of no more than 1 μm (Suter, 2011). Microneedles were attached to a Narishige 3D hydraulic micromanipulator to perform neurite transection on a Nikon TE2000 Eclipse inverted microscope at low magnification (10× phase-contrast objective plus additional 1.5× magnification). For time-lapse imaging experiments, neurite transection and differential interference contrast (DIC) imaging was performed at high magnification (60×1.4 NA oil DIC objective plus additional 1.5× magnification; images captured every 10 s for 110 min; Figure 4d). Neurite transection was carried out at least 100 μm away from the growth cone and at least 100 μm away from the cell body. We only cut a single neurite per neuron. On each coverslip, transection was performed for a subset of neurons, whereas the remaining neurons served as internal control with neurites that were not cut.

In order to measure neurite regeneration rates, we took phase-contrast images with a 10× objective and additional 1.5× magnification right after transection and 4 h later. Neurite length was measured using the segmented line tool of ImageJ, and growth rate of cut and uncut control neurites (neurite length change per hour) was calculated using Microsoft Excel. To reduce the effect of variability between different experiments, growth rates were normalized by the average growth rate of the vehicle-treated uncut control neurites in each experiment (Figure 7).

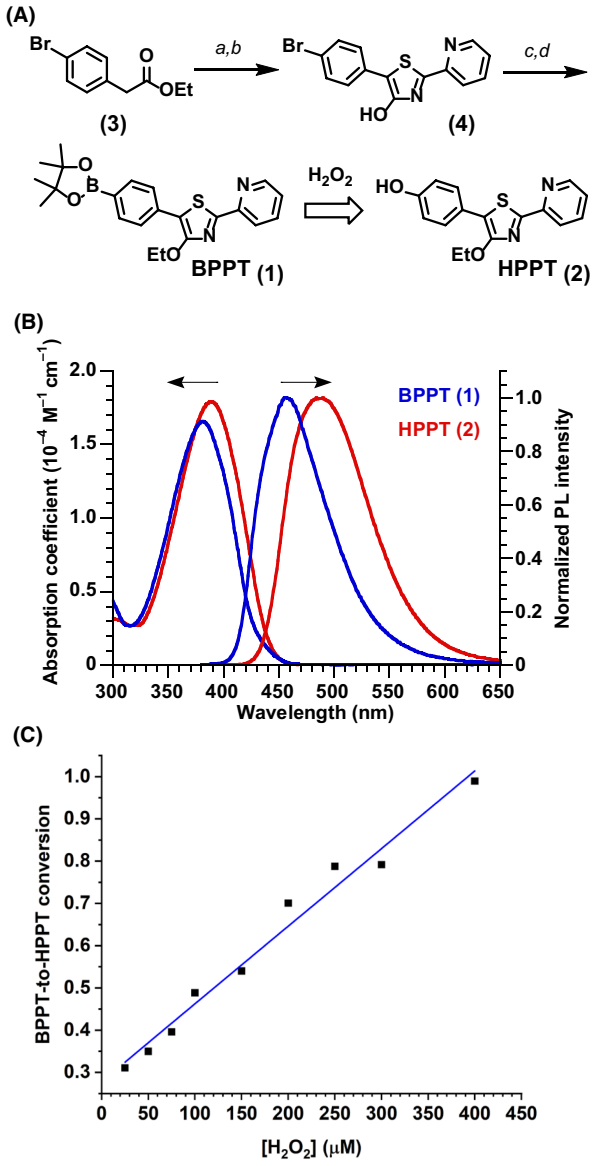

FIGURE 1 Detection of H_2O_2 using BPPT, a novel arylboronate fluorescent probe. (A) Synthetic scheme of BPPT (1) and its oxidation by H_2O_2 into HPPT (2). (a) *N*-bromosuccinimide (NBS), azobisisobutyronitrile (AIBN), α,α,α-trifluorotoluene (TFT), 80°C (84% yield). (b) 2-pyridylthioamide, ethanol, 90°C (microwave) (60% yield). (c) Ethyl iodide, K_2CO_3, acetone, 25°C. (d) Tetrakis(triphenylphosphine)palladium ($Pd(PPh_3)_4$), *bis*(pinacolato) diboron, KOAc, 1,4-dioxane (70% yield over 2 steps). (B) Normalized optical absorption and photoluminescence (PL) spectra of **1** and **2** (in ethanol). (C) Conversion of **1** (1.25 μM in pH 7.8 buffer; λ_{em} 472 nm) into **2** (λ_{em} 540 nm) after 10 min exposure to H_2O_2, as a function of H_2O_2 concentration.

2.3 | Pharmacological experiments

To study the effect of Nox inhibition and ROS reduction on neurite regeneration, we applied celastrol (CST; cat. no. 70950, Cayman Chemical) to the cultures immediately after neurite transection at different final concentrations in L15–ASW medium (CST: 0.1–1.0 μM). CST was prepared as a stock solution in dimethyl sulfoxide (DMSO; 5 mM). For vehicle controls, we applied an appropriate volume of DMSO for the CST study (0.02 v/v% final concentration). To study the effects of CST on BPPT/CRO ratio, CST treatment was done for 20 min before neurite injury (Figure S5). Following the injury, the BPPT and CRO dyes were added to the neurons for 20 min followed by two washes with ASW.

2.4 | Synthesis and characterization of BPPT

5′-(*p*-Borophenyl)-2′-pyridylthiazole pinacol ester (BPPT, **1**) was synthesized in two steps from known compound 5′-*p*-(bromophenyl)-2′-pyridylthiazole (**4**) (Figure 1A; Appendix S1). The pyridylthiazole core was prepared using Hantzsch conditions similar to that described by Beckert and coworkers (Habenicht et al., 2015), followed by 4′-*O*-alkylation and *p*-borylation under Miyaura–Ishiyama conditions (Ishiyama et al., 1995) to yield **1**. An authentic sample of 5′-(*p*-hydroxyphenyl)-2′-pyridylthiazole (HPPT, **2**) was prepared according to our previous report (Watanabe et al., 2020). Chemical reagents and supplies were obtained from commercial sources (Acros Organics, Alfa Aesar, Sigma-Aldrich, and TCI America) unless otherwise noted. Optical absorption and photoluminescence (PL) spectra of BPPT and HPPT were obtained using 30 μM solutions in ethanol and 1.25 or 5 μM solutions in pH 7.8 HEPES buffer. Absorption spectra were acquired on a Varian Cary50 spectrophotometer using a 1-cm quartz cuvette. PL spectra and absolute quantum yields (Φ_{PL}) were measured using an Edinburgh Instruments FLS 980 spectrometer with an integrating sphere accessory.

2.5 | Live cell H_2O_2 imaging

For quantitative H_2O_2 imaging, cultured bag cell neurons were incubated with 4 μM BPPT and 200 nM Calcein Red Orange AM (CRO) (cat. no. C34851, Thermo Fisher Scientific) in ASW for 20 min followed by two washes with ASW to remove excess dye. CRO was used as a cell-permeable fluorescent volume marker for ratiometric H_2O_2 imaging (Davidson & Higgins, 2013; Li et al., 2009; Munnamalai et al., 2014). DIC and fluorescence images were acquired with a 60× 1.4 NA oil objective on a Nikon TE2000E inverted microscope with additional 1.5× magnification, suitable filter sets, and an Andor iXon Ultra 888 EM CCD camera. For BPPT imaging, we used 405/20 nm excitation and 535/40 nm emission filters. For CRO imaging, we used 560/40 nm excitation and 630/60 nm emission filters. In some of the BPPT validation experiments, a second set of images of the same growth cone was acquired 10 min after addition of ASW containing different H_2O_2 concentrations (Figure 3h). In case of neurite transection experiments, BPPT and CRO were applied immediately after in vitro injury. To compare the BPPT localization with a membrane dye, neurons were incubated with 4 μM BPPT and 1 μM DiI (Vybrant™ DiI solution, cat. no. V22885, Thermo Fisher Scientific) in ASW for 20 min. For DiI imaging, we used 560/40 nm excitation and 630/60 nm emission filters (Figure 2d–f). ImageJ was used to measure mean intensity per unit area in the growth cone peripheral (P) domain as well as outside the growth cone (background value). Microsoft Excel was used to calculate the background-subtracted average intensity of each probe in the P domain as well as the ratio of BPPT divided by CRO, which was used as a relative indicator of cytosolic H_2O_2 levels in the growth cone P domain.

2.6 | Nox2/p40^{phox} immunostaining and F-actin labeling

To determine Nox2 and p40^{phox} localization following neurite transection, *Aplysia* bag cell neurons were stained with anti-Nox2 and p40^{phox} antibodies as described previously (Munnamalai et al., 2014). Neurons were fixed with 3.7% formaldehyde solution for 20 min at room temperature (RT), permeabilized with 0.1% saponin in fixation solution for 15 min, washed 3× with PBS/0.01% saponin, and then blocked with 5% bovine serum albumin in PBS/0.01% saponin for 30 min. Fixed cultures were incubated with a rabbit anti-gp91^{phox} antibody R2085 at 1:500 and a mouse anti-p40^{phox} antibody at 1:200 in blocking solution for 1 h at RT. Following three washes with PBS/0.01% saponin, Alexa 488-labeled goat-anti mouse IgG (cat. no. A-11001, Thermo Fisher Scientific) and Alexa 568-labeled goat

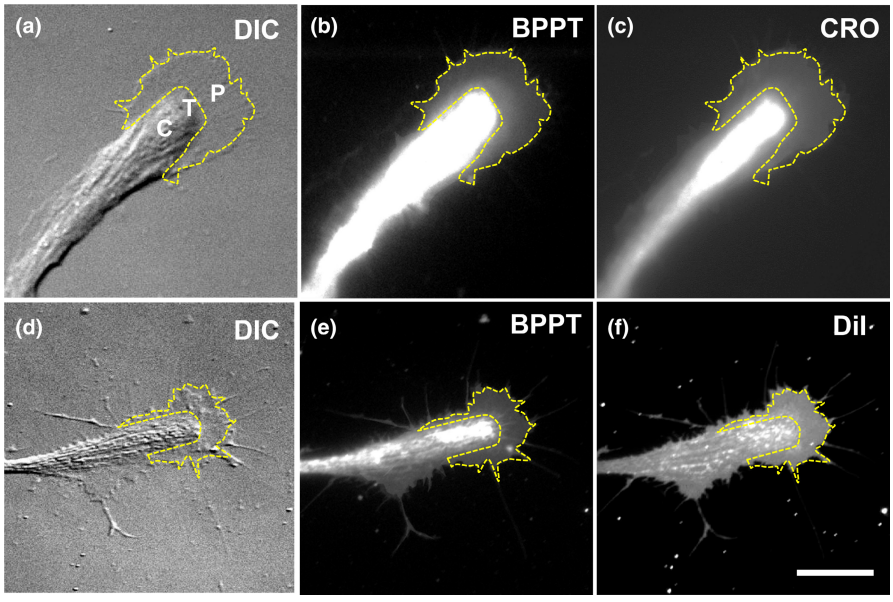

FIGURE 2 BPPT is a H_2O_2-sensitive dye that localizes mostly to the cytoplasm. (a) DIC image of *Aplysia* bag cell neuronal growth cone, indicating locations of P domain (outlined in yellow), T zone, and C domain. Bag cell neuron labeled with BPPT (b) and CRO (c). (d–f) DIC and fluorescence images of neuronal growth cone labeled with BPPT and DiI. The BPPT and CRO intensities are higher in C domain than P domain, whereas the membrane marker DiI labels C and P domains uniformly. Scale bar: 20 μm.

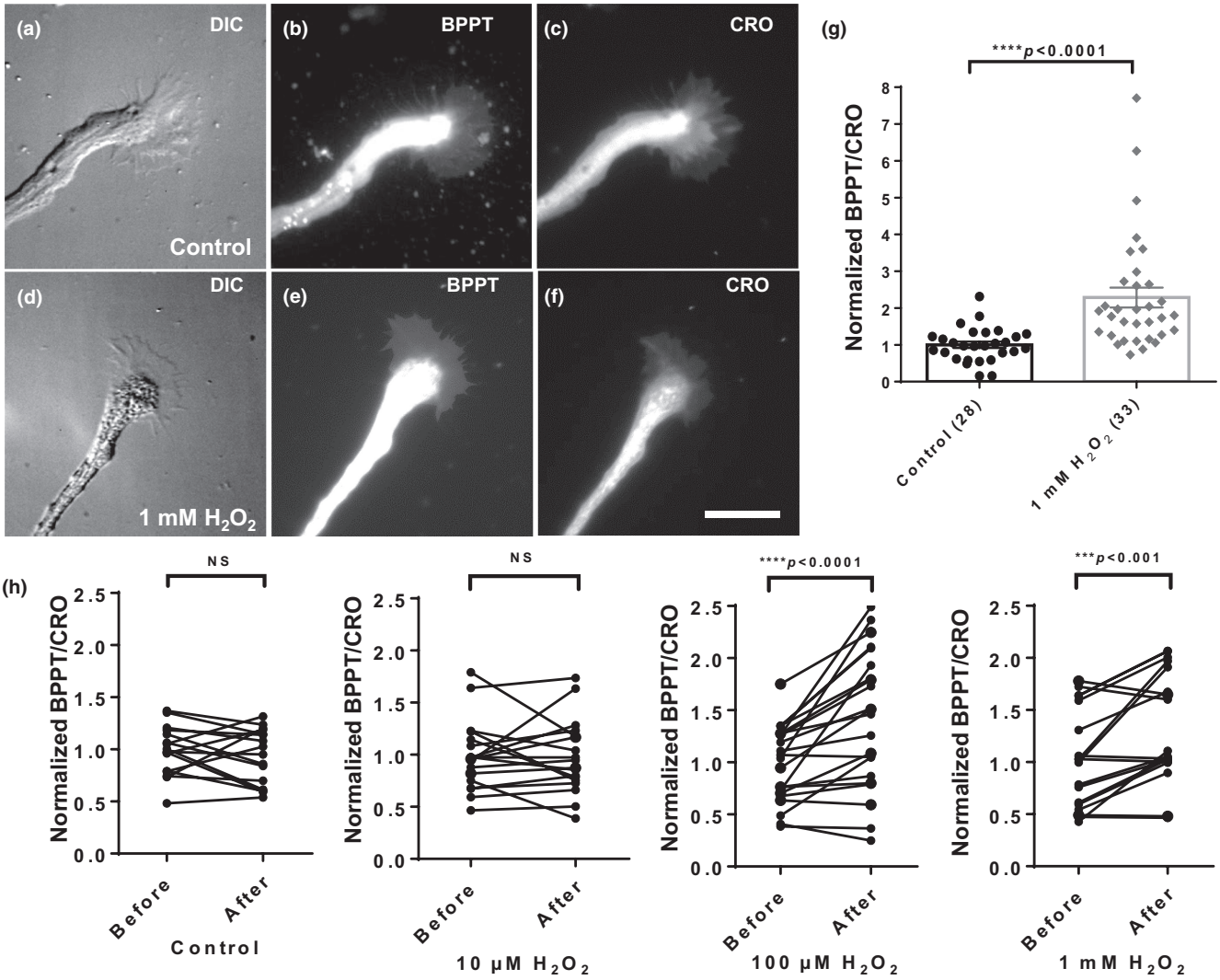

FIGURE 3 Validation of BPPT as H_2O_2-sensitive dye by imaging of live *Aplysia* bag cell growth cones. (a–c) DIC and fluorescence images (BPPT and CRO) of bag cell with growth cone (control; untreated). (d–f) DIC and fluorescence images (BPPT and CRO) of bag cell with growth cone exposed to 1 mM H_2O_2 for 10 min. Scale bar: 20 µm. (g) Treatment with 1 mM H_2O_2 increased intracellular H_2O_2 levels by 129% as measured by normalized BPPT/CRO ratios in the P domain of *Aplysia* bag cell neuronal growth cones. Data for control ($n = 28$) and experiment ($n = 33$) collected from three separate cell platings. (h) Normalized intracellular H_2O_2 levels before and after treatment of growth cones with control solution ($n = 17$) and H_2O_2 at 10 µM ($n = 19$), 100 µM ($n = 23$), and 1 mM H_2O_2 ($n = 19$). Error bars indicate ± SEM. Statistics: D'Agostino–Pearson omnibus normality test; Mann–Whitney non-parametric test (g), $^{****}p < 0.0001$; two-tailed paired *t* test (h); $^{***}p < 0.001$, $^{****}p < 0.0001$.

anti-rabbit IgG antibodies (cat. no. A-11011, Thermo Fisher Scientific) were incubated at 1:250 in blocking solution for 1 h at RT, then washed 3× with PBS/0.01% saponin. For F-actin staining, cells were permeabilized with 1% Triton X-100 in fixation solution for 15 min at RT, washed 3× with PBS/0.1% Triton X-100, incubated with Alexa 568-phalloidin (cat. no. A-12380, Thermo Fisher Scientific) at 1:100 in PBS/0.1% Triton X-100 for 1 h at RT, and washed 3× with PBS/0.1% Triton X-100. Samples were imaged on a Nikon TE2000E inverted microscope equipped with a 60×1.4 NA oil objective plus additional 1.5× magnification and appropriate fluorescence filter sets.

Co-localization analysis of Nox2 and $p40^{phox}$ labeling was performed using the Coloc2 plugin within the Fiji software (Schindelin et al., 2012) by calculating the Pearson's correlation coefficient as performed by Lizama et al. (2018). To mitigate background interference, a rolling-ball background subtraction with a magnitude of 50 was applied. The delineation of neuronal growth cone PT and C domains was achieved with the polygon drawing tool. The point spread function value was set to 1.0, and the Costes randomizations were set to 10.

2.7 | pSrc2/Src2 immunostaining

To determine the levels of activated tyrosine kinase Src2 following neurite transection, *Aplysia* bag cell neurons were labeled with antibodies against *Aplysia* Src2 and activated Src2 (pSrc2) using the

protocol described previously (Decourt et al., 2009; Wu et al., 2008). Briefly, neurons were fixed with 3.7% formaldehyde/400 mM sucrose/ASW for 15 min at RT, permeabilized with 0.1% saponin in fixation solution for 10 min, washed 3× with PBS/0.01% saponin, and then blocked with 10% horse serum in wash buffer (PBS/0.01% saponin) for 30 min. Fixed cells were incubated with a goat anti-Src2 antibody (Wu et al., 2008) at 1:250 and a rabbit anti-pSrc2 antibody (Wu et al., 2008) at 1:250 in blocking solution for 1 h at RT. Following a 3× wash with PBS/0.01% saponin, donkey anti-goat IgG Alexa 568 (cat. no. A-11057, Thermo Fisher Scientific) diluted 1:400 in PBS/0.01% saponin, and goat anti-rabbit IgG Alexa 488 (cat. no. A-11008, Thermo Fisher Scientific) diluted 1:400 in PBS/0.01% saponin were incubated sequentially for 30 min each to avoid cross-reactivity between secondary antibodies. This was followed by three washes with PBS/0.01% saponin. The Nikon TE2000E inverted microscope described earlier was used for imaging. The extent of pSrc2/Src2 was quantified using ImageJ software, namely by measuring mean intensity per unit area in the growth cone peripheral and transition (PT) domain, and C domain, as well as outside the growth cone (background). Microsoft Excel was used to calculate the background-subtracted mean intensity of both pSrc2 and Src2 signals and the pSrc2/Src2 ratio, which was used as a relative indicator of activated Src2 levels in the growth cone.

2.8 | Statistical analysis

Data were analyzed using GraphPad Prism 6.0 software. The number (n) of samples indicated in the figures is the number of growth cones analyzed from at least 2–3 independent *Aplysia* bag cell platings. The number of samples and experiments were based on our previous experience with this model system. No power analysis was performed before the experiment. Outliers were identified and removed using ROUT ($Q = 1\%$) method. Outliers were removed in the following datasets: Figure 3g (2 outliers), Figure 3h (5 outliers), Figure 5 (3 outliers), and Figure 7 (8 outliers). Data normality was assessed using the D'Agostino–Pearson omnibus test and $p < 0.05$ was considered significant. In most cases, data were normalized against the mean value of the control group. Bars in each graph show mean value ± standard error of the mean along with dots for individual data point. For all pairwise comparison a Student's t test (paired or unpaired based on the dataset) was used if the data are normally distributed, otherwise non-parametric tests were used. Datasets containing multiple treatment groups were also analyzed by multigroup comparison. Detailed statistical information for all figures with quantifications is provided in the supplementary information.

3 | RESULTS

3.1 | BPPT – A novel H_2O_2-imaging dye

The field of ROS signaling is limited by the availability of fluorescent probes that are both specific to individual ROS molecules and exhibit a linear response over a large dynamic range (Sies et al., 2022). Pyridylthiazoles with 4-alkoxy substituents produce fluorescence at visible wavelengths with remarkably high quantum yields (Grummt et al., 2007), and are an excellent scaffold for designing donor–π–acceptor (D–π–A) systems that produce stimuli-responsive emission shifts. We recently introduced 5′-(*p*-hydroxyphenyl)-2′-pyridylthiazole (HPPT, **2**) as a highly emissive D–π–A fluorophore having a large Stokes shift, with further shifts in emission wavelength possible by installing a chemical recognition unit (Watanabe et al., 2020). HPPT has good solubility in water, which prompted us to consider its use as a fluorescent indicator for H_2O_2 by oxidation of a suitable arylboronate precursor, namely BPPT (**1**; Figure 1). Specifically, we anticipated an increase in intramolecular charge transfer upon oxidation of **1** into **2** by H_2O_2 (Figure 1A) accompanied by a sizable redshift in

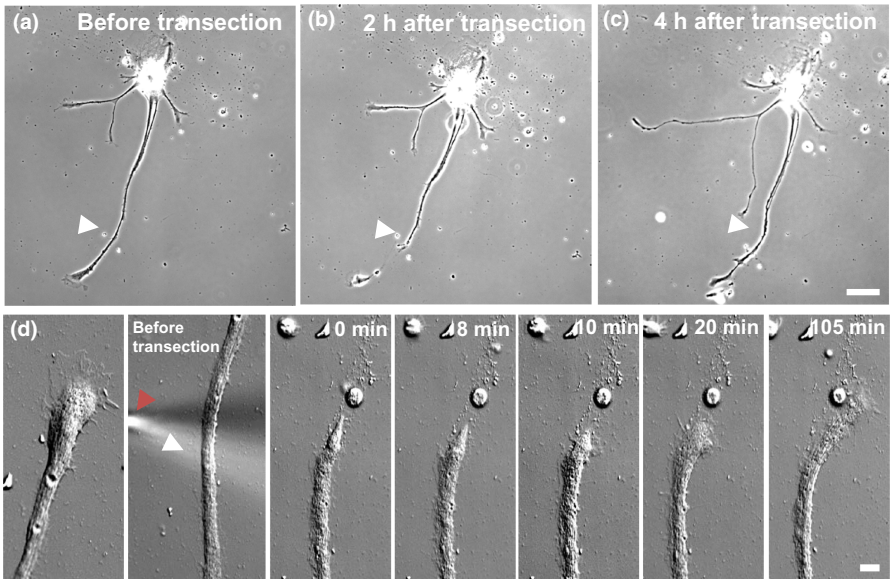

FIGURE 4 In vitro transection of *Aplysia* bag cell neurons followed by neurite regeneration. (a) Bag cell neuron with neurite just prior to transection by microneedle; location of cut is marked with white arrowhead. (b, c) 2 and 4 h after transection, respectively; the distal neurite has re-grown from the initial cut site. Scale bar: 100 μm. (d) High-magnification (90×) DIC images of regenerating neurite after injury at select time points. Cut location is marked with white arrowhead; glass needle tip is marked with a red arrowhead. A new growth cone at the tip of the cut neurite is observed within 10–20 min. Scale bar: 10 μm.

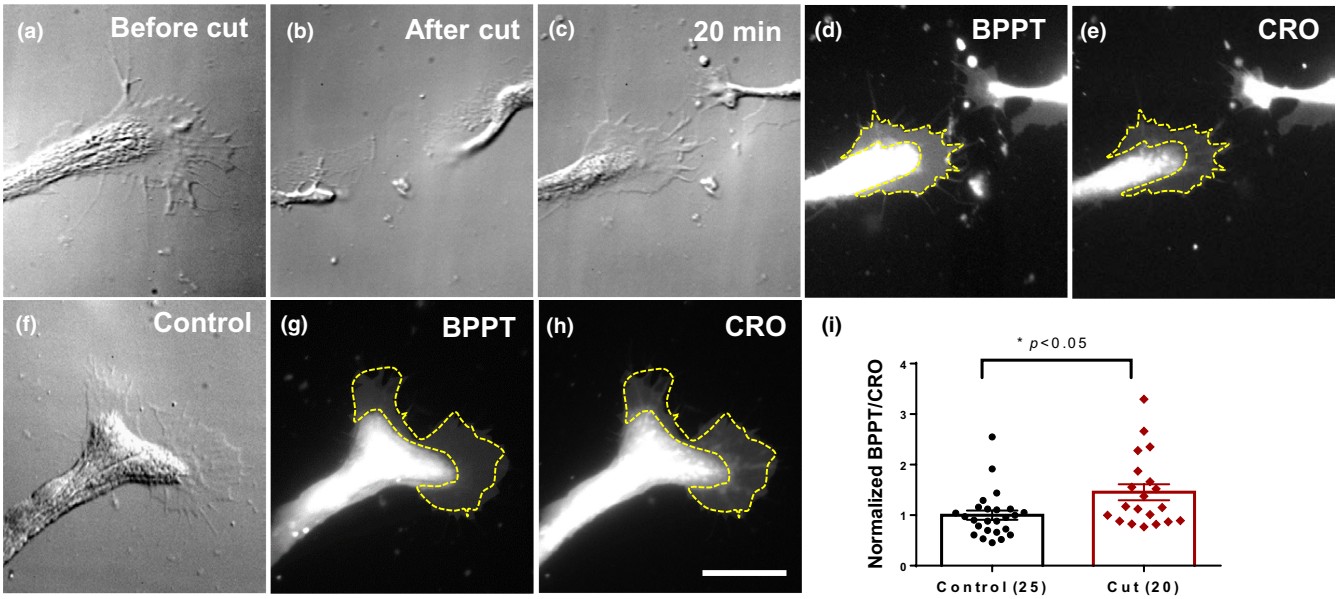

FIGURE 5 H_2O_2 levels in regenerating growth cones are elevated following neurite transection. DIC images of growth cone before (a), immediately after (b), and 20 min after neurite transection (c). (d, e) Fluorescence images (BPPT and CRO) of regenerating growth cone shown in (c). (f–h) Images of control growth cone for comparison. Scale bar: 10 μm. (i) Neurite transection significantly increased H_2O_2 levels in the P domain of regenerating growth cones by 45%. Data for control ($n = 25$) and cut neurites ($n = 20$) collected from five separate cell platings. Error bars indicate ± SEM. Statistical test: two-tailed Mann–Whitney; $^*p < 0.05$.

emission (Figure 1B), which was confirmed by photoluminescence (PL) spectroscopy (Figure S2) and ESI-MS analysis (Figure S3).

BPPT has a strong absorption band near 380 nm (π–π^* transition) that is blue shifted relative to that of HPPT ($\lambda_{max} = 388$ nm), attributable to a reduction in π-electron density by the boronate unit. Likewise, **1** in ethanol exhibits a peak fluorescence (λ_{em}) at 456 nm that is blue shifted relative to **2** by 31 nm ($\lambda_{em} = 487$ nm) due to large differences in D–π–A character (Figure 1B). The PL quantum yields (Φ_{PL}) of **1** and **2** in ethanol are both close to 90%, in accord with our previous studies (Figure S1, Table S1) (Watanabe et al., 2020). Treatment of **1** with H_2O_2 caused a redshift in λ_{em} by 28 nm in ethanol (Figure S2a) and by 34 nm in aqueous solutions at pH 7.8, with some modest reduction in fluorescence peak intensity (Figure S2b,c). The kinetics of BPPT oxidation at pH 7.8 were determined to be first order with respect to both **1** (below 2.5 μM) and H_2O_2, with the linear range of H_2O_2 detection starting at 25 μM (Figure 1C). The sensitivity of **1** to superoxide and other reactive oxygen species has yet to be characterized, though it is worth mentioning that HPPT can react with superoxide anion to generate a novel intermediate. However, this does not affect our fluorescence analysis as superoxide disproportionates rapidly into H_2O_2. In conclusion, our in vitro characterization shows that BPPT is a H_2O_2-sensitive dye.

3.2 | Measuring H_2O_2 in *Aplysia* bag cell growth cones using BPPT

In order to quantify H_2O_2 in growth cones of cultured *Aplysia* bag cell neurons, we applied BPPT as a H_2O_2-sensing dye and calcein red–orange AM (CRO) as a volume marker for ratiometric imaging (Figure 2). We focused our analysis on the thin growth cone P domain for three reasons: (i) changes in cytoplasmic H_2O_2 levels are more likely detectable in the P domain because baseline BPPT signals are lower in the P than in the C domain, (ii) the P domain is the largest area of the growth cone and therefore likely contains the most membrane receptors to initiate H_2O_2 production, and (iii) fluorescent signals are significantly higher and thus more difficult to quantify in the C domain and the neurite because of the high density of organelles such as mitochondria, which have high ROS levels (Figure 2b,c). By comparing BPPT signal intensity with the volume indicator dye CRO and membrane indicator dye DiI, we found BPPT to be mostly localized to the cytoplasm (Figure 2). Both BPPT and CRO signals were homogenously distributed in the thin P domain of the growth cones but were significantly lower relative to the levels in the C domain and neurite. On the other hand, DiI was distributed uniformly across the growth cone P and C domain and neurite, as expected for a membrane-associated dye. We thus find that BPPT distributes largely to the cytoplasm of *Aplysia* neurons.

Next, we tested the H_2O_2-sensing property of BPPT in *Aplysia* bag cell growth cones by exposing cultured neurons to different concentrations of H_2O_2 for 10 min (Figure 3). Exposure to 1 mM H_2O_2 increased the mean ratiometric BPPT/CRO fluorescence intensity in the P domain by 129% when compared to control growth cones without H_2O_2 (Figure 3g). By applying different concentrations of H_2O_2 (10 μM, 100 μM, and 1 mM) and measuring BPPT and CRO emissions before and after H_2O_2 application, we found a significant increase in BPPT/CRO ratios for treatments with 100 μM ($p < 0.0001$) and 1 mM H_2O_2 ($p < 0.001$; Figure 3h). When analyzing the BPPT and CRO

intensities before and after treatment with H_2O_2 in more detail, we noticed that in average both dyes exhibited slightly reduced intensities when the second image was acquired during control treatment (Figure S4). Treatment with 1 mM H_2O_2 did not significantly increase the average BPPT intensity but decreased the average CRO intensity ($p < 0.0001$), possibly because of volume effects by H_2O_2 or reaction with CRO. The BPPT/CRO ratio significantly increased after treatment with 1 mM H_2O_2 ($p < 0.001$), indicating that there is a positive correlation between cellular H_2O_2 levels and BPPT/CRO ratio. This confirms that BPPT is a H_2O_2-sensitive dye, whose distribution is largely commensurate with cytoplasmic volume.

3.3 | Neurite transection increases intracellular H_2O_2 levels

We used an in vitro *Aplysia* neurite transection model previously established to study cellular events after nerve injury (Gitler & Spira, 1998; Spira et al., 1996) to investigate the role of Nox and H_2O_2 in neurite regeneration. After culturing *Aplysia* bag cell neurons for 48 h, we employed a sharp microneedle to transect a single neurite per neuron at least 100 μm away from the cell body and at least 100 μm away from the growth cone. We observed that the distal end of the neurite connected with the cell body formed a bulb and started to degenerate immediately after transection (Figure 4; Video S1). Within 10 min, a new growth cone formed at the tip of the cut neurite, a signature of regeneration (Figure 4). This was observed for approximately 80% of all cut neurites.

To determine H_2O_2 levels in growth cones of regenerating neurites, we performed ratiometric BPPT/CRO imaging 20 min after injury (Figure 5a–e). These measurements indicated that H_2O_2 levels in the P domain of regenerating growth cones increased by 45%, a significant change relative to growth cones of uninjured neurites (Control; Figure 5f–i). This result suggests that the in vitro transection of *Aplysia* bag cell neurites elevates intracellular H_2O_2 concentrations in regenerating growth cones.

3.4 | Redistribution of Nox2 and p40 in the growth cone C domain after injury

Association of cytosolic regulatory subunits with the main membrane-bound Nox2 enzyme indicates activation of the Nox2 complex (Brandes et al., 2014; Rastogi et al., 2017). We previously reported that cellular stimulation with the *Aplysia* adhesion molecule apCAM increases $p40^{phox}$ co-localization with Nox2 in *Aplysia* bag cell growth cones (Munnamalai et al., 2014). To determine potential changes in the activation state of Nox2, we performed Nox2 and $p40^{phox}$ double immunostaining after in vitro neurite transection (Figure 6). We noticed a redistribution of Nox2 and $p40^{phox}$ after injury suggestive of increased co-localization (Figure 6e,f). Foci of Nox2/$p40^{phox}$ co-localization are marked with arrows in the magnified color overlays shown in Figure 6c',f'. Quantification of the co-localization was performed by calculating the Pearson's correlation coefficient. Indeed, we found a small but significant increase of co-localization in the C domain of regenerating growth cones ($n = 23$) relative to control growth cones ($n = 47$) ($p < 0.05$; Figure 6h) but did not observe any significant changes in Nox2/$p40^{phox}$ co-localization in the growth cone P domain and T zone (Figure 6g). These results are in accordance with our findings on higher H_2O_2 levels in regenerating growth cones following neurite transection, which suggests that Nox2 is activated in regenerating growth cones after injury.

3.5 | Nox activity is required for neurite regeneration

To determine whether Nox activity is required for neurite regeneration following mechanical transection, we treated cultured bag cell neurons with celastrol (CST), a potent pan-Nox inhibitor known to inhibit Nox1, Nox2, Nox4, and Nox5 (Jaquet et al., 2011). After neurite transection, bag cells were treated with different concentrations of CST (0.1, 0.5, and 1 μM), and regeneration was monitored for 4 h after injury using phase-contrast imaging at low magnification (Figure 7). A set of cells was also treated with DMSO as a vehicle control, using the same volume as in CST treatments. We have found in previous studies that DMSO does not significantly alter neurite growth rates when applied at 0.1 v/v% or less (Munnamalai et al., 2014); in this study, the average growth rate of uncut (DMSO-treated) neurites was 20 ± 3.9 μm/h, whereas the growth rate of regenerating (cut) neurites increased by 43% ($p < 0.05$, two-tailed unpaired *t* test). The growth rates of both control and regenerating neurites were significantly reduced by both 0.5 and 1 μM CST ($p < 0.0001$; two-tailed unpaired *t* test; Figure 7). These results suggest that Nox activity is required for neurite regeneration following mechanical injury.

To study the effects of CST on H_2O_2 levels using BPPT/CRO imaging, 1 μM CST treatment was performed for 20 min before the initiation of neurite injury (Figure S5). Following the injury, the BPPT and CRO dye was added to the neurons for 20 min followed by two washes with ASW. We found a statistically significant fourfold reduction in BPPT/CRO fluorescence intensity ratio in CST-treated regenerating compared to untreated regenerating growth cones ($p < 0.01$; two-tailed unpaired *t* test). Similarly, growth cones that remained uncut exhibited a significant 2.5-fold reduction in BPPT/CRO ratio because of CST treatment ($p < 0.001$; two-tailed unpaired *t* test).

3.6 | Nox inhibition affects growth cone morphology and F-actin content in regenerating neurites

To investigate the effects of Nox inhibition on the morphology and F-actin organization of growth cones at the tip of regenerating

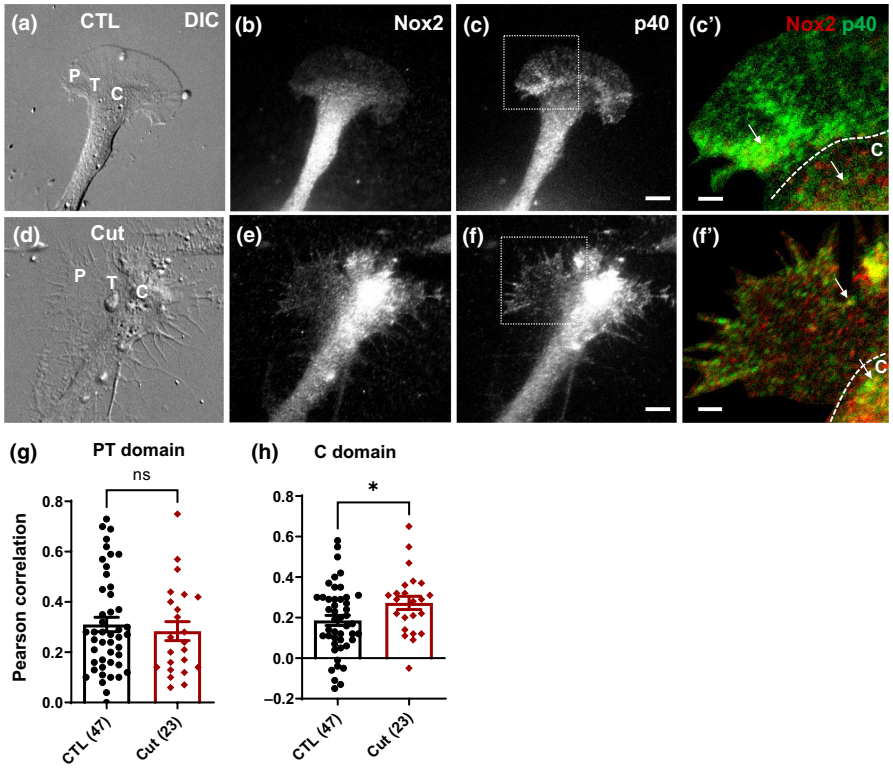

FIGURE 6 In vitro injury causes redistribution of $p40^{phox}$ and Nox2. (a) DIC image of an uninjured (control, CTL) growth cone; P domain, T zone, and C domain are labeled. Immunofluorescence images for Nox2 (b) and $p40^{phox}$ (c). (c') Magnified view of region of interest boxed in (c) shown as color overlay of Nox2 (red) and $p40^{phox}$ (green). Arrows point to foci of co-localization. C domain boundary is marked with a dashed line. (d–f) Images of a regenerating growth cone after in vitro transection. (f') Magnified view of region of interest boxed in (f) shown as color overlay. Scale bars: 10 μm in (c) and (f); 5 μm in (c') and (f'). Quantification of $p40^{phox}$/Nox2 co-localization in the P domain and T zone (g) and C domain (h) by calculating the Pearson's correlation coefficient. Increased $p40^{phox}$/Nox2 co-localization is observed in the C domain following injury compared to uncut controls, but not in the P domain or T zone. Data shown for control ($n = 47$) and cut neurons ($n = 23$) collected from two separate cell platings. Average values ± SEM are shown. Statistics: Two-tailed unpaired Student's *t* test; $^{*}p < 0.05$.

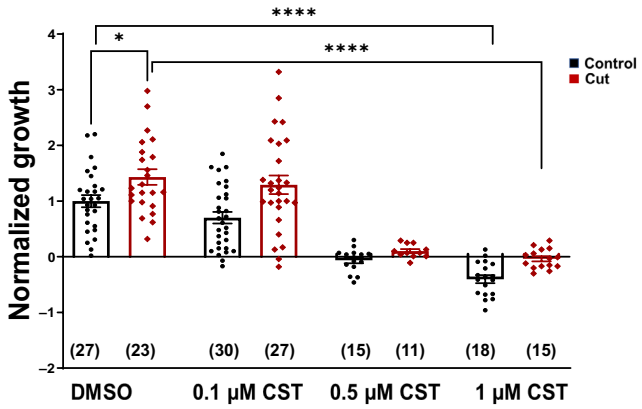

FIGURE 7 Growth rates of regenerating neurites are reduced by Nox inhibition. Regenerating neurites following mechanical transection grew faster than control neurites that were not transected, following treatment with DMSO alone ($p < 0.05$). Treatment with CST reduced both control and regenerative neurite growth completely at and above 0.5 μM CST. Two-tailed unpaired Student's *t* test; $^{*}p < 0.05$, $^{****}p < 0.0001$. Detailed statistics are provided in the supplementary information.

neurites, we performed high-resolution F-actin and DIC imaging following fixation and phalloidin staining (Figure 8). We previously reported that Nox inhibition by VAS2870 and CST flattened the P domain and transition (T) zone of growth cones and reduced neurite growth (Munnamalai et al., 2014). In the same study, we also showed that VAS2870 treatment reduced the F-actin content of *Aplysia* bag cell growth cones. To test whether Nox inhibition by CST has similar effects on growth cones of regenerating neurites, we treated bag cell neurons with 1 μM CST for 20 min. We found that CST treatment reduced the F-actin content in control growth cones of uninjured (DMSO-treated) neurites, in accord with our previous findings (Figure 8a–d). Regenerating growth cones of cut neurites were generally smaller and had a less organized F-actin cytoskeleton in the P domain with fewer filopodial bundles when compared to control growth cones (Figure 8e,f). CST-treated growth cones of regenerating neurites also exhibited a flat T zone and P domain with reduced F-actin content when compared with control growth cones (Figure 8g,h). In conclusion, Nox activity is required for neurite outgrowth and F-actin organization in the growth cones of both uninjured and regenerating neurites.

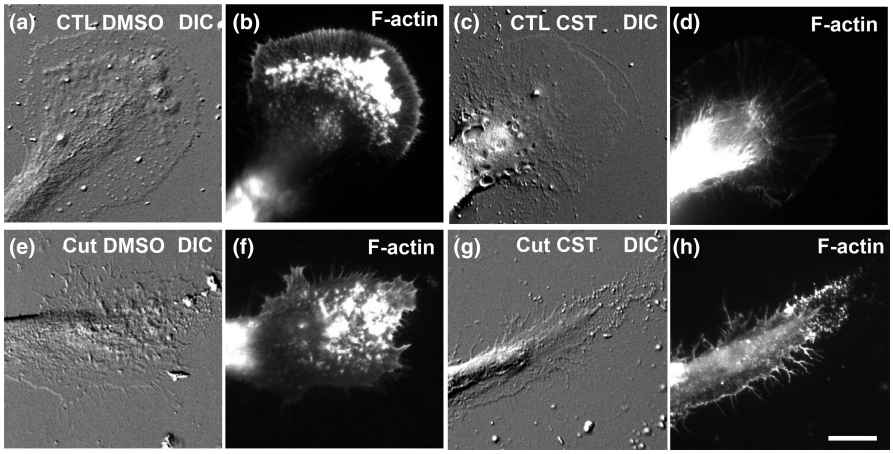

FIGURE 8 Nox inhibitor CST reduces F-actin content in *Aplysia* bag cell growth cone. (a, b) High magnification DIC and Alexa 568-phalloidin images of a control (CTL) growth cone treated with DMSO. The P domain shows the typical radial array of filopodial F-actin bundles. (c, d) Same set of images of a growth cone treated with 1 μM CST for 20 min. CST treatment caused flattening of growth cone T zone and P domain and reduction of F-actin content. (e, f) High magnification DIC and Alexa 568-phalloidin images of a regenerating growth cone following neurite transection. The F-actin in the P domain is not as organized as in untransected control growth cones. (g, h) Same set of images of a regenerating growth cone treated with 1 μM CST for 20 min. In vitro injury and CST treatment reduced the F-actin content and affected the F-actin organization in the growth cones. Scale bar: 20 μm.

3.7 | Nox inhibition affects the Src2 tyrosine kinase activation state in the growth cone

Based on our previous reports, Src tyrosine kinase regulates the morphology and dynamics of lamellipodia and filopodia in *Aplysia* bag cell growth cones (He et al., 2015; Wu et al., 2008). Src family kinase proteins contain redox-sensitive conserved cysteine residues in the SH2 and kinase domains and can be regulated by ROS (Giannoni et al., 2005; Heppner, 2021). Src activity regulates several downstream effector proteins such as cortactin, which control actin organization and dynamics (Ren et al., 2019; Tehrani et al., 2007). To test whether Src tyrosine kinase is a potential downstream effector of Nox in neuronal growth cones, we investigated the effect of pharmacological Nox inhibition on the Src2 activation state (Figure 9). Therefore, we stained regenerating and CST-treated growth cones with specific antibodies against activated (pSrc2) and total Src2 (Wu et al., 2008) and determined the pSrc2/Src2 ratio in both the PT domain (P domain and T zone combined) and C domain (Figure 9a–l), which is indicative of the Src2 activation state. We found that in vitro injury triggers a higher Src2 activation state in the growth cone P domain and T zone of regenerating neurites compared to uncut controls (two-tailed unpaired *t* test, $p < 0.05$; Figure 9m). In the C domain, a modest increase in pSrc2/Src2 ratio was also observed (Figure 9n). Bag cell neurons were treated with 1 μM CST for 20 min immediately after injury, followed by immunostaining and visualization of the growth cone. The pSrc2/Src2 levels in the C domain of uninjured control and injured neurites were both significantly reduced by 1 μM CST (two-tailed Mann–Whitney exact test, $p < 0.05$ and <0.005, respectively; Figure 9n), whereas no significant reduction was detected in the P domain or T zone. These findings suggest that (i) in vitro injury triggers a higher Src2 activation state in *Aplysia* bag cell growth cones and (ii) Nox activity affects the level of the Src2 activation state in the growth cones of both uninjured and regenerating neurites.

4 | DISCUSSION

Our study is the first to show that neuronal Nox activity is required for neurite regeneration after in vitro mechanical injury at the single-cell level. Increased H_2O_2 generation and higher Nox2/$p40^{phox}$ co-localization in regenerating growth cones strongly indicate that neurite transection induces higher Nox activity. Pharmacological interference with the pan-Nox inhibitor celastrol slowed neurite regeneration rates, suggesting neuronal Nox-derived H_2O_2 to be critical for neurite regeneration following injury. This is in agreement with earlier reports on normal neurite growth of cultured neurons (Munnamalai et al., 2014; Wilson et al., 2015). In the course of this research, we also designed and validated BPPT, a novel H_2O_2-sensitive fluorochrome with high quantum efficiency that undergoes a 30-nm shift in emission wavelength upon reaction with H_2O_2. This is the first description of BPPT, a fluorescent pyridylthiazole that converts to HPPT upon reaction with H_2O_2. While we found a linear response of BPPT to H_2O_2 in vitro, this was not observed when exposing growth cones to increasing H_2O_2 concentrations. We suspect H_2O_2 reduction by cytosolic redox-defense systems to be a factor in this apparently non-linear relationship observed in cells.

Nox and Nox-derived ROS are widely recognized for their harmful role in traumatic CNS injury and neurodegenerative disorders (Lee et al., 2021; Ma et al., 2017). ROS levels are elevated following SCI (Xu et al., 2005) along with increased expression and activity of various Nox isoforms in microglia, astrocytes, and neurons (Cooney et al., 2014; Kim et al., 2010; Vaziri et al., 2004; von Leden et al., 2017). Nox2 expression is up-regulated in both

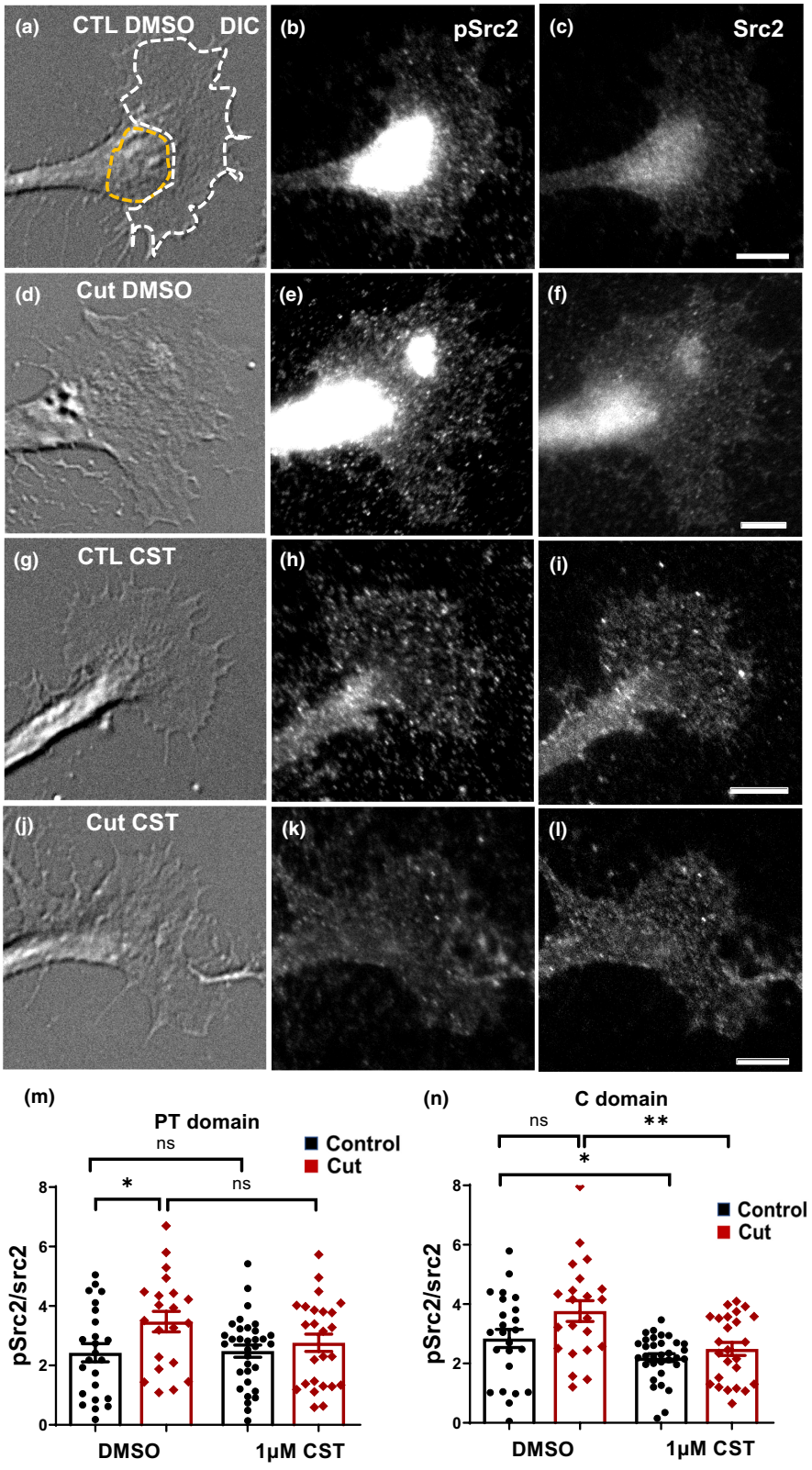

FIGURE 9 Nox inhibitor CST reduces the Src2 activation state in *Aplysia* growth cone. (a–c) Control growth cone without transection and treated with vehicle (DMSO) was immunolabeled for pSrc2 (b) and Src2 (c). Outlined regions in (a) represent P domain and T zone (white dashed line) and C domain (orange dashed line). (d–f) Corresponding images of a regenerating growth cone. (g–i) Control growth cone without transection but treated with 1 μM CST for 20 min. (j–l) Corresponding images of a regenerating and CST-treated growth cone. Scale bar: 10 μm. (m, n) Quantification of pSrc2/Src2 ratio in the growth cone P domain and T zone (m) and C domain (n). Average values ± SEM shown for control/DMSO ($n = 24$), cut/DMSO ($n = 22$), control/CST ($n = 33$), and cut/CST ($n = 25$). Data are from three separate cell platings. We found a higher pSrc2/Src2 ratio following injury when compared to uninjured controls in the P domain and T zone (two-tailed unpaired *t* test, $^{*}p < 0.05$). CST treatment reduced pSrc2/Src2 in the growth cone C domain for both uncut control (two-tailed Mann–Whitney exact test, $^{*}p < 0.05$), and injured neurites (two-tailed Mann–Whitney exact test, $^{**}p < 0.005$) compared to the corresponding DMSO-treated control or cut growth cones, respectively.

neurons and glial cells, especially in microglia after SCI (Cooney et al., 2014; von Leden et al., 2017). Nox inhibition has neuroprotective and anti-inflammatory effects and can contribute to partial recovery from injury in SCI animal models (Impellizzeri et al., 2011; Khayrullina et al., 2015; Sun et al., 2017). Similarly, Nox-derived ROS in microglia cause neurological damage after traumatic brain injury (Dohi et al., 2010), and lack of Nox2 correlates with improved recovery after brain injury (Lo et al., 2007).

Aside from the damaging role of Nox-derived ROS in diseases and injury, Nox enzymes also have a wide variety of physiological

functions in numerous cell and tissue types (Bedard & Krause, 2007; Vermot et al., 2021). Nox has been implicated in different aspects of neuronal development including neurogenesis, neuronal polarity, and axonal growth (Terzi & Suter, 2020; Wilson et al., 2018). Thus, it appears that an intermediate levels of Nox activity and ROS is optimal for normal nervous system physiology. There is also increasing evidence that Nox regulates axonal regeneration; however, the specific cellular source of Nox and Nox-derived H_2O_2 is not fully understood. Duox1-derived H_2O_2 and keratinocytes are critical for the regeneration of peripheral axons following fin amputation in larval zebrafish (Rieger & Sagasti, 2011). Similarly, CRISPR/Cas9-generated *duox* mutant zebrafish larvae exhibit reduced CNS regeneration after laser-mediated injury of Mauthner cell axons (Yang et al., 2020). Nox2 has also been implicated in regeneration of sensory axons as demonstrated with the mouse conditioned lesioning system (De Virgiliis et al., 2020; Hervera et al., 2018).

The role of Nox in axonal regeneration following injury is complex, given its involvement in both axonal degeneration and regeneration as well as its up-regulation in glial cells and neurons. For these reasons, we used *Aplysia* bag cell neurons, a very well-defined system, to investigate Nox-mediated neurite regeneration in vitro. *Aplysia* neurons are an excellent model system to study basic cellular mechanisms of neurite growth and synaptic plasticity, which are highly conserved throughout evolution. Furthermore, several homologs of genes associated with human neurological diseases have been identified in the *Aplysia* genome; thus, *Aplysia* neurons are a valuable model system to investigate molecular and cellular mechanisms of neurological diseases (Walters & Moroz, 2009). Cultured *Aplysia* neurons have been used previously to study the resealing of transected axons (Spira et al., 1996) as well as the mechanism of growth cone formation following in vitro injury (Gitler & Spira, 1998). Here, we found that *Aplysia* bag cell neurons have a high capacity for neurite regeneration without additional treatments. In our study, approximately 80% of cut neurites could be regenerated within 20 min if transections were performed at least 100 μm away from the cell body (Figure 4, Video S1). Distal neurites formed a bulb that initially retracted following mechanical transection, followed by the formation of a new growth cone, which advanced in a similar direction as before. We also found that the growth rate of regenerating neurites was 43% higher relative to uninjured ones (Figure 7). Increased growth rates of regenerating neurites correlated with elevated H_2O_2 levels in the growth cone P domain (Figure 5). Does H_2O_2 promote regeneration of bag cell neurites? It has been previously shown using hippocampal cell lines that H_2O_2 increases neurite outgrowth (Min et al., 2006; Shimoda et al., 2021). To determine whether Nox2 activation is responsible for increased H_2O_2 levels in regenerating neurites, we performed Nox2/p40^{phox} double labeling and observed increased co-localization in the C domain following injury, though it remained constant in the P domain. These results suggest that Nox2 activation occurs in the C domain of the regenerating growth cone, with subsequent elevation of H_2O_2 levels in the P domain.

To determine whether Nox activity is required for axonal regeneration, we treated bag cell neurons with cut and uninjured neurites with different concentrations of the pan-Nox inhibitor CST (Figure 7). We found that higher concentrations of CST significantly reduced neurite growth rates of both regenerating and normally growing neurites, whereas low concentrations had no significant effects. This is in agreement with our previous studies with *Aplysia* neurons (Munnamalai et al., 2014) and cultured zebrafish retinal ganglion cells (Weaver et al., 2018), in which CST treatment inhibited basic neurite outgrowth. Our results indicate that neuronal Nox activity is required for neurite regeneration. Unfortunately, we are not able to determine the contribution of specific Nox isoforms to regeneration in *Aplysia* neurons, since we do not have the necessary tools available. CST has been previously used for its neuroprotective and anti-inflammatory effects after traumatic CNS injury and in a variety of neuropathological conditions in order to reduce oxidative stress induced by up-regulated Nox (Kiaei et al., 2005; Liu et al., 2021); however, the exact mechanism of how this compound acts has remained unclear. Furthermore, there are no major breakthroughs in clinical trials of antioxidant therapy for human SCI patients. This is likely because of the Janus-faced role of Nox and derived ROS in axonal degeneration and regeneration. The findings from our studies suggest that optimal dosing of Nox inhibitors may improve axonal regeneration following SCI.

What are the potential downstream effectors of Nox-derived H_2O_2 signaling in axonal regeneration? The most widely studied and accepted mechanism for Nox regulation involves the oxidation of cysteine residues. There are several redox-sensitive signaling molecules and regulatory proteins that ultimately affect cytoskeletal and membrane dynamics as well as gene expression (Balta et al., 2020; Terzi & Suter, 2020). Nox-derived H_2O_2 modifies cysteine or methionine residues of redox-sensitive proteins thereby changing their activity (Finkel, 2011). Redox-sensitive effector proteins involved in axonal growth and regeneration include the ryanodine receptor (Wilson et al., 2016), Rho GTPases (Hobbs et al., 2014), inositol phosphatase PTEN (Hervera et al., 2018), Src tyrosine kinase (Gianoni et al., 2005), PKG1 (Valek et al., 2017), and actin (Grintsevich et al., 2016). PTEN is an interesting target protein for redox signaling in axonal regeneration, as its deletion is known to improve axonal regeneration after CNS injury (Liu et al., 2010; Park et al., 2008). PTEN counteracts PI3-kinase signaling, which in turn promotes axonal regeneration in adult CNS (Nieuwenhuis et al., 2020; Nieuwenhuis & Eva, 2022). Nox2 mediates axonal regeneration of mouse DRG neurons in vivo through PTEN oxidation and activation of the PI3-kinase signaling pathway (Hervera et al., 2018). PI3-kinase signaling can alter actin and microtubule dynamics in several different ways.

In this study, we provide evidence that Nox inhibition reduces F-actin content in regenerating growth cones (Figure 8). To elucidate the potential downstream effectors of Nox-mediated actin organization and neuronal regeneration, we examined the possible link between Nox and Src tyrosine kinase activity in the *Aplysia* bag cell growth cone. Src tyrosine kinase is a redox-sensitive protein (Heppner et al., 2018) that can regulate actin dynamics in neuronal growth cones (He et al., 2015). We found a significantly higher level of Src2 activation state in the growth cone P and T domain after injury where we detected elevated H_2O_2 levels (Figure 9).

Pharmacological inhibition of Nox caused reduced pSrc2/Src2 ratio in the growth cone C domain in both control and injured neurites (Figure 9). This suggests a possible role of Src tyrosine kinase as a downstream effector of Nox that regulates actin-mediated neurite outgrowth and regeneration. The large *Aplysia* growth cone provides an excellent system to further dissect the cellular mechanisms of how Nox-derived ROS promote neurite regeneration following mechanical injury.

AUTHOR CONTRIBUTIONS

S. M. Sabbir Alam, Yuichiro Watanabe, Alexander Wei, and Daniel M. Suter designed the study. S. M. Sabbir Alam, Yuichiro Watanabe, Brooke L. Steeno, Soumyajit Dutta, and Halie A. Szilagyi performed experiments. S. M. Sabbir Alam, Yuichiro Watanabe, Brooke L. Steeno, Soumyajit Dutta, Alexander Wei, and Daniel M. Suter were involved with data analysis. S. M. Sabbir Alam, Yuichiro Watanabe, Alexander Wei, and Daniel M. Suter wrote or edited the manuscript.

ACKNOWLEDGMENTS

We are thankful to Dr. Mark Quinn (Montana State University) for providing us with Nox2 and $p40^{phox}$ antibodies. This project was supported, in part, by the Indiana Spinal Cord & Brain Injury Research Fund from the Indiana State Department of Health (Contract 26351) and by a grant from NIH (5R01NS117701). Y.W. gratefully acknowledges a fellowship provided by the Japan Society for the Promotion of Science (JSPS). A.W. gratefully acknowledges the ACS Petroleum Research Fund (58453-ND4). We thank Patricia Bishop and Hartmut Hedderich for technical support.

All experiments were conducted in compliance with the ARRIVE guidelines.

CONFLICT OF INTEREST STATEMENT

The authors do not have any conflicts of interest.

PEER REVIEW

The peer review history for this article is available at https://www.webofscience.com/api/gateway/wos/peer-review/10.1111/jnc.15977.

DATA AVAILABILITY STATEMENT

The data that support the findings of this study are available from the corresponding author upon reasonable request. Custom-made materials will be shared upon request.

ORCID

Yuichiro Watanabe https://orcid.org/0000-0001-7521-0983
Halie A. Szilagyi https://orcid.org/0000-0003-1564-2770
Daniel M. Suter https://orcid.org/0000-0002-5230-7229

REFERENCES

Ahuja, C. S., Wilson, J. R., Nori, S., Kotter, M. R. N., Druschel, C., Curt, A., & Fehlings, M. G. (2017). Traumatic spinal cord injury. *Nature Reviews. Disease Primers*, *3*, 17018.

Anjum, A., Yazid, M. D., Fauzi Daud, M., Idris, J., Ng, A. M. H., Selvi Naicker, A., Ismail, O. H. R., Athi Kumar, R. K., & Lokanathan, Y. (2020). Spinal cord injury: Pathophysiology, multimolecular interactions, and underlying recovery mechanisms. *International Journal of Molecular Sciences*, *21*, 7533.

Athamneh, A. I. M., He, Y., Lamoureux, P., Fix, L., Suter, D. M., & Miller, K. E. (2017). Neurite elongation is highly correlated with bulk forward translocation of microtubules. *Scientific Reports*, *7*, 7292.

Balta, E., Kramer, J., & Samstag, Y. (2020). Redox regulation of the Actin cytoskeleton in cell migration and adhesion: On the way to a spatiotemporal view. *Frontiers in Cell and Development Biology*, *8*, 618261.

Bedard, K., & Krause, K. H. (2007). The NOX family of ROS-generating NADPH oxidases: Physiology and pathophysiology. *Physiological Reviews*, *87*, 245–313.

Brandes, R. P., Weissmann, N., & Schroder, K. (2014). Nox family NADPH oxidases: Molecular mechanisms of activation. *Free Radical Biology & Medicine*, *76*, 208–226.

Chang, M. C., Pralle, A., Isacoff, E. Y., & Chang, C. J. (2004). A selective, cell-permeable optical probe for hydrogen peroxide in living cells. *Journal of the American Chemical Society*, *126*, 15392–15393.

Cooney, S. J., Zhao, Y., & Byrnes, K. R. (2014). Characterization of the expression and inflammatory activity of NADPH oxidase after spinal cord injury. *Free Radical Research*, *48*, 929–939.

Davidson, A. F., & Higgins, A. Z. (2013). Detection of volume changes in calcein-stained cells using confocal microscopy. *Journal of Fluorescence*, *23*, 393–398.

De Virgiliis, F., Hutson, T. H., Palmisano, I., Amachree, S., Miao, J., Zhou, L., Todorova, R., Thompson, R., Danzi, M. C., Lemmon, V. P., Bixby, J. L., Wittig, I., Shah, A. M., & Di Giovanni, S. (2020). Enriched conditioning expands the regenerative ability of sensory neurons after spinal cord injury via neuronal intrinsic redox signaling. *Nature Communications*, *11*, 6425.

Decourt, B., Munnamalai, V., Lee, A. C., Sanchez, L., & Suter, D. M. (2009). Cortactin colocalizes with filopodial actin and accumulates at IgCAM adhesion sites in *Aplysia* growth cones. *Journal of Neuroscience Research*, *87*, 1057–1068.

Dickinson, B. C., Peltier, J., Stone, D., Schaffer, D. V., & Chang, C. J. (2011). Nox2 redox signaling maintains essential cell populations in the brain. *Nature Chemical Biology*, *7*, 106–112.

Dohi, K., Ohtaki, H., Nakamachi, T., Yofu, S., Satoh, K., Miyamoto, K., Song, D., Tsunawaki, S., Shioda, S., & Aruga, T. (2010). Gp91phox (NOX2) in classically activated microglia exacerbates traumatic brain injury. *Journal of Neuroinflammation*, *7*, 41.

Finkel, T. (2011). Signal transduction by reactive oxygen species. *The Journal of Cell Biology*, *194*, 7–15.

Giannoni, E., Buricchi, F., Raugei, G., Ramponi, G., & Chiarugi, P. (2005). Intracellular reactive oxygen species activate Src tyrosine kinase during cell adhesion and anchorage-dependent cell growth. *Molecular and Cellular Biology*, *25*, 6391–6403.

Gitler, D., & Spira, M. E. (1998). Real time imaging of calcium-induced localized proteolytic activity after axotomy and its relation to growth cone formation. *Neuron*, *20*, 1123–1135.

Grintsevich, E. E., Yesilyurt, H. G., Rich, S. K., Hung, R. J., Terman, J. R., & Reisler, E. (2016). F-actin dismantling through a redox-driven synergy between Mical and cofilin. *Nature Cell Biology*, *18*, 876–885.

Grummt, U. W., Weiss, D., Birckner, E., & Beckert, R. (2007). Pyridylthiazoles: Highly luminescent heterocyclic compounds. *The Journal of Physical Chemistry. A*, *111*, 1104–1110.

Habenicht, S. H., Schramm, S., Zhu, M., Freund, R. R., Langenstück, T., Strathausen, R., Weiß, D., Biskup, C., & Beckert, R. (2015). π-Extension of a 4-ethoxy-1, 3-thiazole via aryl alkyne cross coupling: Synthesis and exploration of the electronic structure. *Photochemical & Photobiological Sciences*, *14*, 2097–2107.

Hall, E. D. (2011). Antioxidant therapies for acute spinal cord injury. *Neurotherapeutics*, *8*, 152–167.

He, Y., Ren, Y., Wu, B., Decourt, B., Lee, A. C., Taylor, A., & Suter, D. M. (2015). Src and cortactin promote lamellipodia protrusion and filopodia formation and stability in growth cones. *Molecular Biology of the Cell*, *26*, 3229–3244.

Heppner, D. E. (2021). Structural insights into redox-active cysteine residues of the Src family kinases. *Redox Biology*, *41*, 101934.

Heppner, D. E., Dustin, C. M., Liao, C., Hristova, M., Veith, C., Little, A. C., Ahlers, B. A., White, S. L., Deng, B., Lam, Y. W., Li, J., & van der Vliet, A. (2018). Direct cysteine sulfenylation drives activation of the Src kinase. *Nature Communications*, *9*, 1–11.

Hervera, A., De Virgiliis, F., Palmisano, I., Zhou, L., Tantardini, E., Kong, G., Hutson, T., Danzi, M. C., Perry, R. B., Santos, C. X. C., Kapustin, A. N., Fleck, R. A., Del Río, J. A., Carroll, T., Lemmon, V., Bixby, J. L., Shah, A. M., Fainzilber, M., & Di Giovanni, S. (2018). Reactive oxygen species regulate axonal regeneration through the release of exosomal NADPH oxidase 2 complexes into injured axons. *Nature Cell Biology*, *20*, 307–319.

Hobbs, G. A., Zhou, B., Cox, A. D., & Campbell, S. L. (2014). Rho GTPases, oxidation, and cell redox control. *Small GTPases*, *5*, e28579.

Impellizzeri, D., Mazzon, E., Esposito, E., Paterniti, I., Bramanti, P., & Cuzzocrea, S. (2011). Effect of Apocynin, an inhibitor of NADPH oxidase, in the inflammatory process induced by an experimental model of spinal cord injury. *Free Radical Research*, *45*, 221–236.

Ishiyama, T., Murata, M., & Miyaura, N. (1995). Palladium(0)-catalyzed cross-coupling reaction of alkoxydiboron with haloarenes: A direct procedure for arylboronic esters. *The Journal of Organic Chemistry*, *60*, 7508–7510.

Jaquet, V., Marcoux, J., Forest, E., Leidal, K. G., McCormick, S., Westermaier, Y., Perozzo, R., Plastre, O., Fioraso-Cartier, L., Diebold, B., Scapozza, L., Nauseef, W. M., Fieschi, F., Krause, K. H., & Bedard, K. (2011). NADPH oxidase (NOX) isoforms are inhibited by celastrol with a dual mode of action. *British Journal of Pharmacology*, *164*, 507–520.

Kawahara, T., Quinn, M. T., & Lambeth, J. D. (2007). Molecular evolution of the reactive oxygen-generating NADPH oxidase (Nox/Duox) family of enzymes. *BMC Evolutionary Biology*, *7*, 109.

Khayrullina, G., Bermudez, S., & Byrnes, K. R. (2015). Inhibition of NOX2 reduces locomotor impairment, inflammation, and oxidative stress after spinal cord injury. *Journal of Neuroinflammation*, *12*, 172.

Kiaei, M., Kipiani, K., Petri, S., Chen, J., Calingasan, N. Y., & Beal, M. F. (2005). Celastrol blocks neuronal cell death and extends life in transgenic mouse model of amyotrophic lateral sclerosis. *Neurodegenerative Diseases*, *2*, 246–254.

Kim, D., You, B., Jo, E. K., Han, S. K., Simon, M. I., & Lee, S. J. (2010). NADPH oxidase 2-derived reactive oxygen species in spinal cord microglia contribute to peripheral nerve injury-induced neuropathic pain. *Proceedings of the National Academy of Sciences of the United States of America*, *107*, 14851–14856.

Lee, S. H., Lee, M., Ko, D. G., Choi, B. Y., & Suh, S. W. (2021). The role of NADPH oxidase in neuronal death and neurogenesis after acute neurological disorders. *Antioxidants*, *10*, 739.

Li, L., Hutchins, B. I., & Kalil, K. (2009). Wnt5a induces simultaneous cortical axon outgrowth and repulsive axon guidance through distinct signaling mechanisms. *The Journal of Neuroscience*, *29*, 5873–5883.

Lippert, A. R., Van de Bittner, G. C., & Chang, C. J. (2011). Boronate oxidation as a bioorthogonal reaction approach for studying the chemistry of hydrogen peroxide in living systems. *Accounts of Chemical Research*, *44*, 793–804.

Liu, D.-D., Luo, P., Gu, L., Zhang, Q., Gao, P., Zhu, Y., Chen, X., Guo, Q., Zhang, J., Ma, N., & Wang, J. (2021). Celastrol exerts a neuroprotective effect by directly binding to HMGB1 protein in cerebral ischemia–reperfusion. *Journal of Neuroinflammation*, *18*, 174.

Liu, K., Lu, Y., Lee, J. K., Samara, R., Willenberg, R., Sears-Kraxberger, I., Tedeschi, A., Park, K. K., Jin, D., Cai, B., Xu, B., Connolly, L., Steward, O., Zheng, B., & He, Z. (2010). PTEN deletion enhances the regenerative ability of adult corticospinal neurons. *Nature Neuroscience*, *13*, 1075–1081.

Lizama, B. N., Palubinsky, A. M., Raveendran, V. A., Moore, A. M., Federspiel, J. D., Codreanu, S. G., Liebler, D. C., & McLaughlin, B. (2018). Neuronal preconditioning requires the mitophagic activity of C-terminus of HSC70-interacting protein. *The Journal of Neuroscience*, *38*, 6825–6840.

Lo, W., Bravo, T., Jadhav, V., Titova, E., Zhang, J. H., & Tang, J. (2007). NADPH oxidase inhibition improves neurological outcomes in surgically-induced brain injury. *Neuroscience Letters*, *414*, 228–232.

Ma, M. W., Wang, J., Zhang, Q., Wang, R., Dhandapani, K. M., Vadlamudi, R. K., & Brann, D. W. (2017). NADPH oxidase in brain injury and neurodegenerative disorders. *Molecular Neurodegeneration*, *12*, 7.

Magnani, F., Nenci, S., Fananas, E. M., Ceccon, M., Romero, E., Fraaije, M. W., & Mattevi, A. (2017). Crystal structures and atomic model of NADPH oxidase. *Proceedings of the National Academy of Sciences of the United States of America*, *114*, 6764–6769.

Meda, F., Gauron, C., Rampon, C., Teillon, J., Volovitch, M., & Vriz, S. (2016). Nerves control redox levels in mature tissues through Schwann cells and hedgehog signaling. *Antioxidants & Redox Signaling*, *24*, 299–311.

Min, J. Y., Park, M. H., Park, M. K., Park, K. W., Lee, N. W., Kim, T., Kim, H. J., & Lee, D. H. (2006). Staurosporin induces neurite outgrowth through ROS generation in HN33 hippocampal cell lines. *Journal of Neural Transmission*, *113*, 1821–1826.

Moghadam, Z. M., Henneke, P., & Kolter, J. (2021). From flies to men: ROS and the NADPH oxidase in phagocytes. *Frontiers in Cell and Development Biology*, *9*, 628991.

Munnamalai, V., & Suter, D. M. (2009). Reactive oxygen species regulate F-actin dynamics in neuronal growth cones and neurite outgrowth. *Journal of Neurochemistry*, *108*, 644–661.

Munnamalai, V., Weaver, C. J., Weisheit, C. E., Venkatraman, P., Agim, Z. S., Quinn, M. T., & Suter, D. M. (2014). Bidirectional interactions between NOX2-type NADPH oxidase and the F-actin cytoskeleton in neuronal growth cones. *Journal of Neurochemistry*, *130*, 526–540.

Nayernia, Z., Jaquet, V., & Krause, K.-H. (2014). New insights on NOX enzymes in the central nervous system. *Antioxidants & Redox Signaling*, *20*, 2815–2837.

Nieuwenhuis, B., Barber, A. C., Evans, R. S., Pearson, C. S., Fuchs, J., MacQueen, A. R., van Erp, S., Haenzi, B., Hulshof, L. A., Osborne, A., Conceicao, R., Khatib, T. Z., Deshpande, S. S., Cave, J., Ffrench-Constant, C., Smith, P. D., Okkenhaug, K., Eickholt, B. J., Martin, K. R., … Eva, R. (2020). PI 3-kinase delta enhances axonal PIP3 to support axon regeneration in the adult CNS. *EMBO Molecular Medicine*, *12*, e11674.

Nieuwenhuis, B., & Eva, R. (2022). Promoting axon regeneration in the central nervous system by increasing PI3-kinase signaling. *Neural Regeneration Research*, *17*, 1172–1182.

Park, K. K., Liu, K., Hu, Y., Smith, P. D., Wang, C., Cai, B., Xu, B., Connolly, L., Kramvis, I., Sahin, M., & He, Z. (2008). Promoting axon regeneration in the adult CNS by modulation of the PTEN/mTOR pathway. *Science*, *322*, 963–966.

Rastogi, R., Geng, X., Li, F., & Ding, Y. (2017). NOX activation by subunit interaction and underlying mechanisms in disease. *Frontiers in Cellular Neuroscience*, *10*, 301.

Ren, Y., He, Y., Brown, S., Zbornik, E., Mlodzianoski, M. J., Ma, D., Huang, F., Mattoo, S., & Suter, D. M. (2019). A single tyrosine phosphorylation site in cortactin is important for filopodia formation in neuronal growth cones. *Molecular Biology of the Cell*, *30*, 1817–1833.

Rieger, S., & Sagasti, A. (2011). Hydrogen peroxide promotes injury-induced peripheral sensory axon regeneration in the zebrafish skin. *PLoS Biology*, *9*, e1000621.

Schindelin, J., Arganda-Carreras, I., Frise, E., Kaynig, V., Longair, M., Pietzsch, T., Preibisch, S., Rueden, C., Saalfeld, S., Schmid, B.,

Tinevez, J. Y., White, D. J., Hartenstein, V., Eliceiri, K., Tomancak, P., & Cardona, A. (2012). Fiji: An open-source platform for biological-image analysis. *Nature Methods*, *9*, 676–682.

Shimoda, A., Tanabe, T., Sato, T., & Nedachi, T. (2021). Hydrogen peroxide induces progranulin expression to control neurite outgrowth in HT22 cells. *Bioscience, Biotechnology, and Biochemistry*, *85*, 2103–2112.

Sies, H., Belousov, V. V., Chandel, N. S., Davies, M. J., Jones, D. P., Mann, G. E., Murphy, M. P., Yamamoto, M., & Winterbourn, C. (2022). Defining roles of specific reactive oxygen species (ROS) in cell biology and physiology. *Nature Reviews. Molecular Cell Biology*, *23*, 499–515.

Sikora, A., Zielonka, J., Dębowska, K., Michalski, R., Smulik-Izydorczyk, R., Pięta, J., Podsiadły, R., Artelska, A., Pierzchała, K., & Kalyanaraman, B. (2020). Boronate-based probes for biological oxidants: A novel class of molecular tools for redox biology. *Frontiers in Chemistry*, *8*, 580899.

Spira, M. E., Dormann, A., Ashery, U., Gabso, M., Gitler, D., Benbassat, D., Oren, R., & Ziv, N. E. (1996). Use of *Aplysia* neurons for the study of cellular alterations and the resealing of transected axons in vitro. *Journal of Neuroscience Methods*, *69*, 91–102.

Sun, Y., Gong, F., Yin, J., Wang, X., Wang, X., Sun, Q., Zhu, Z., Su, X., Zheng, J., Liu, L., Li, Y., Hu, X., & Li, J. (2017). Therapeutic effect of apocynin through antioxidant activity and suppression of apoptosis and inflammation after spinal cord injury. *Experimental and Therapeutic Medicine*, *13*, 952–960.

Suter, D. M. (2011). Live cell imaging of neuronal growth cone motility and guidance in vitro. *Methods in Molecular Biology*, *769*, 65–86.

Tehrani, S., Tomasevic, N., Weed, S., Sakowicz, R., & Cooper, J. A. (2007). Src phosphorylation of cortactin enhances actin assembly. *Proceedings of the National Academy of Sciences of the United States of America*, *104*, 11933–11938.

Terzi, A., Roeder, H., Weaver, C. J., & Suter, D. M. (2021). Neuronal NADPH oxidase 2 regulates growth cone guidance downstream of slit2/robo2. *Developmental Neurobiology*, *81*, 3–21.

Terzi, A., & Suter, D. M. (2020). The role of NADPH oxidases in neuronal development. *Free Radical Biology & Medicine*, *154*, 33–47.

Valek, L., Haussler, A., Drose, S., Eaton, P., Schroder, K., & Tegeder, I. (2017). Redox-guided axonal regrowth requires cyclic GMP dependent protein kinase 1: Implication for neuropathic pain. *Redox Biology*, *11*, 176–191.

Vaziri, N. D., Lee, Y. S., Lin, C. Y., Lin, V. W., & Sindhu, R. K. (2004). NAD(P)H oxidase, superoxide dismutase, catalase, glutathione peroxidase and nitric oxide synthase expression in subacute spinal cord injury. *Brain Research*, *995*, 76–83.

Vermot, A., Petit-Härtlein, I., Smith, S. M. E., & Fieschi, F. (2021). NADPH oxidases (NOX): An overview from discovery, molecular mechanisms to physiology and pathology. *Antioxidants*, *10*, 890.

von Leden, R. E., Yauger, Y. J., Khayrullina, G., & Byrnes, K. R. (2017). Central nervous system injury and nicotinamide adenine dinucleotide phosphate oxidase: Oxidative stress and therapeutic targets. *Journal of Neurotrauma*, *34*, 755–764.

Walters, E. T., & Moroz, L. L. (2009). Molluscan memory of injury: Evolutionary insights into chronic pain and neurological disorders. *Brain, Behavior and Evolution*, *74*, 206–218.

Watanabe, Y., Sungnoi, W., Sartorio, A. O., Zeller, M., & Wei, A. (2020). A zinc-responsive fluorophore based on 5′-(p-hydroxyphenyl)-pyridyl thiazole. *Materials Chemistry Frontiers*, *4*, 899–904.

Weaver, C. J., Terzi, A., Roeder, H., Gurol, T., Deng, Q., Leung, Y. F., & Suter, D. M. (2018). nox2/cybb deficiency affects zebrafish retinotectal connectivity. *The Journal of Neuroscience*, *38*, 5854–5871.

Wilson, C., Munoz-Palma, E., & Gonzalez-Billault, C. (2018). From birth to death: A role for reactive oxygen species in neuronal development. *Seminars in Cell & Developmental Biology*, *80*, 43–49.

Wilson, C., Muñoz-Palma, E., Henríquez, D. R., Palmisano, I., Núñez, M. T., Di Giovanni, S., & González-Billault, C. (2016). A feed-forward mechanism involving the NOX complex and RyR-mediated Ca^{2+} release during axonal specification. *The Journal of Neuroscience*, *36*, 11107–11119.

Wilson, C., Nunez, M. T., & Gonzalez-Billault, C. (2015). Contribution of NADPH oxidase to the establishment of hippocampal neuronal polarity in culture. *Journal of Cell Science*, *128*, 2989–2995.

Wu, B., Decourt, B., Zabidi, M. A., Wuethrich, L. T., Kim, W. H., Zhou, Z., MacIsaac, K., & Suter, D. M. (2008). Microtubule-mediated Src tyrosine kinase trafficking in neuronal growth cones. *Molecular Biology of the Cell*, *19*, 4611–4627.

Xu, W., Chi, L., Xu, R., Ke, Y., Luo, C., Cai, J., Qiu, M., Gozal, D., & Liu, R. (2005). Increased production of reactive oxygen species contributes to motor neuron death in a compression mouse model of spinal cord injury. *Spinal Cord*, *43*, 204–213.

Yang, L. Q., Chen, M., Ren, D. L., & Hu, B. (2020). Dual oxidase mutant retards Mauthner-cell axon regeneration at an early stage via modulating mitochondrial dynamics in zebrafish. *Neuroscience Bulletin*, *36*, 1500–1512.

Zielonka, J., Sikora, A., Hardy, M., Joseph, J., Dranka, B. P., & Kalyanaraman, B. (2012). Boronate probes as diagnostic tools for real time monitoring of peroxynitrite and hydroperoxides. *Chemical Research in Toxicology*, *25*, 1793–1799.

SUPPORTING INFORMATION

Additional supporting information can be found online in the Supporting Information section at the end of this article.

How to cite this article: Alam, S. M. S., Watanabe, Y., Steeno, B. L., Dutta, S., Szilagyi, H. A., Wei, A., & Suter, D. M. (2023). Neuronal NADPH oxidase is required for neurite regeneration of *Aplysia* bag cell neurons. *Journal of Neurochemistry*, *00*, 1–15. https://doi.org/10.1111/jnc.15977